Supporting Information

Steering the Methane Dry Reforming Reactivity of Ni/La_2O_3 Catalysts by Controlled *In Situ* Decomposition of doped La_2NiO_4 Precursor Structures

Maged F. Bekheet,[1] Parastoo Delir Kheyrollahi Nezhad,[2,3] Nicolas Bonmassar[3], Lukas Schlicker[1], Albert Gili[1], Sebastian Praetz,[4] Aleksander Gurlo[1], Andrew Doran[5], Yuanxu Gao[6], Marc Heggen[6], Aligholi Niaei,[2] Ali Farzi,[2] Sabine Schwarz,[7] Johannes Bernardi[7], Bernhard Klötzer[3] and Simon Penner[3,*]

[1]*Fachgebiet Keramische Werkstoffe/Chair of Advanced Ceramic Materials, Institut für Werkstoffwissenschaften und -technologien, Technische Universität Berlin, Hardenbergstr. 40, 10623 Berlin, Germany*

[2]*Reactor & Catalyst Research Lab, Department of Chemical Engineering, University of Tabriz, Tabriz, Iran*

[3]*Department of Physical Chemistry, University of Innsbruck, Innrain 52c, A-6020 Innsbruck, Austria*

[4] *Institute of Optics and Atomic Physics, Technische Universität Berlin, Hardenbergstraße 36, 10623 Berlin, Germany*

[5]*Advanced Light Source, Lawrence Berkeley National Laboratory Berkeley, California 94720, USA*

[6]*Ernst Ruska-Centrum für Mikroskopie und Spektroskopie mit Elektronen Forschungszentrum Jülich GmbH52425 Jülich, Germany*

[7]*University Service Center for Transmission Electron Microscopy, TU Wien, Wiedner Hauptstrasse 8-10, A-1040 Vienna, Austria*

*Corresponding Author: simon.penner@uibk.ac.at, Tel: 004351250758003, Fax: 004351250758199

Section A: BET analysis

Table S1: BET surface area (m^2g^{-1}) of the four catalysts before and after catalytic DRM at 800 °C for 90 min, obtained from 5 point measurements recorded at 77 K after degassing the samples under vacuum for 10 h at 200 °C.

Sample	**Before DRM**	**After DRM**
$La_2Ni_{0.9}Cu_{0.1}O_4$	3.252	4.241
$La_2Ni_{0.8}Cu_{0.2}O_4$	2.218	3.896
$La_{1.8}Ba_{0.2}Ni_{0.9}Cu_{0.1}O_4$	3.695	4.748
$La_{1.8}Ba_{0.2}NiO_4$	4.549	3.021

Section B: Electron microscopy analysis of $La_{1.8}Ba_{0.2}NiO_4$ and $La_{1.8}Ba_{0.2}Ni_{0.9}Cu_{0.1}O_4$ in the states before and after DRM at 800 °C.

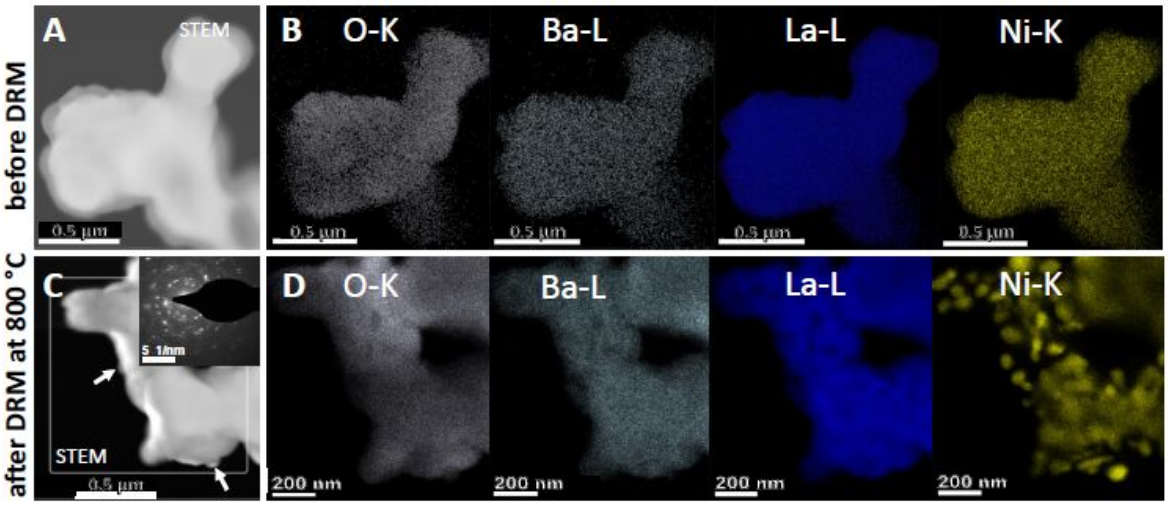

Figure S1: Electron microscopy analysis of $La_{1.8}Ba_{0.2}NiO_4$ in the initial and DRM-spent state at 800 °C. Panels A and C: HAADF images, Panels B and D: EDX analysis of the O-K, Ba-L, La-L and Ni-K.

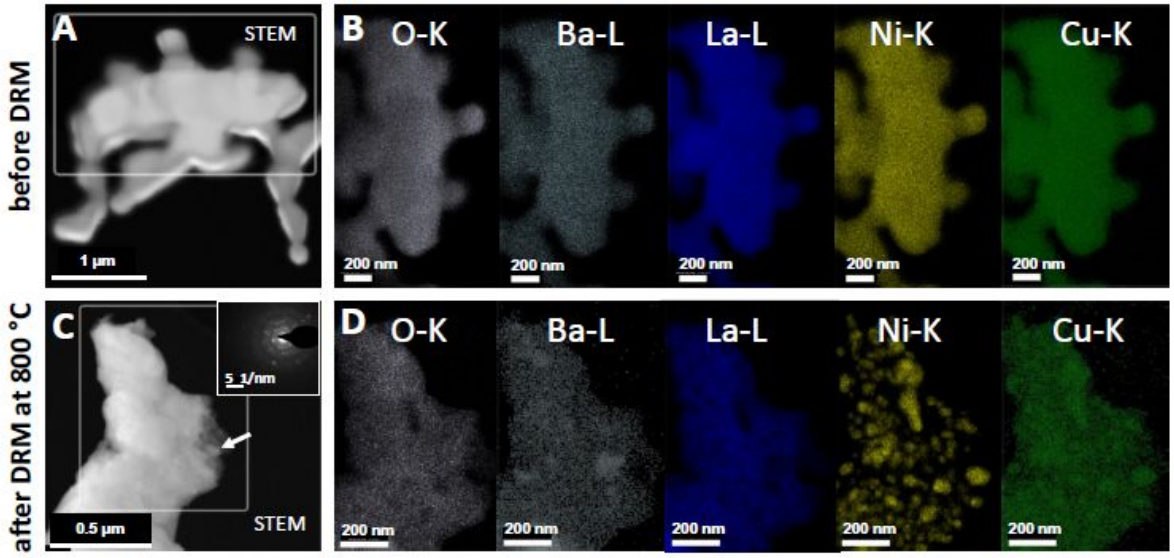

Figure S2: Electron microscopy analysis of $La_{1.8}Ba_{0.2}Ni_{0.9}Cu_{0.1}O_4$ in the initial and DRM-spent state at 800 °C. Panels A and C: HAADF images, Panels B and D: EDX analysis of the O-K, Ba-L, La-L, Cu-K and Ni-K.

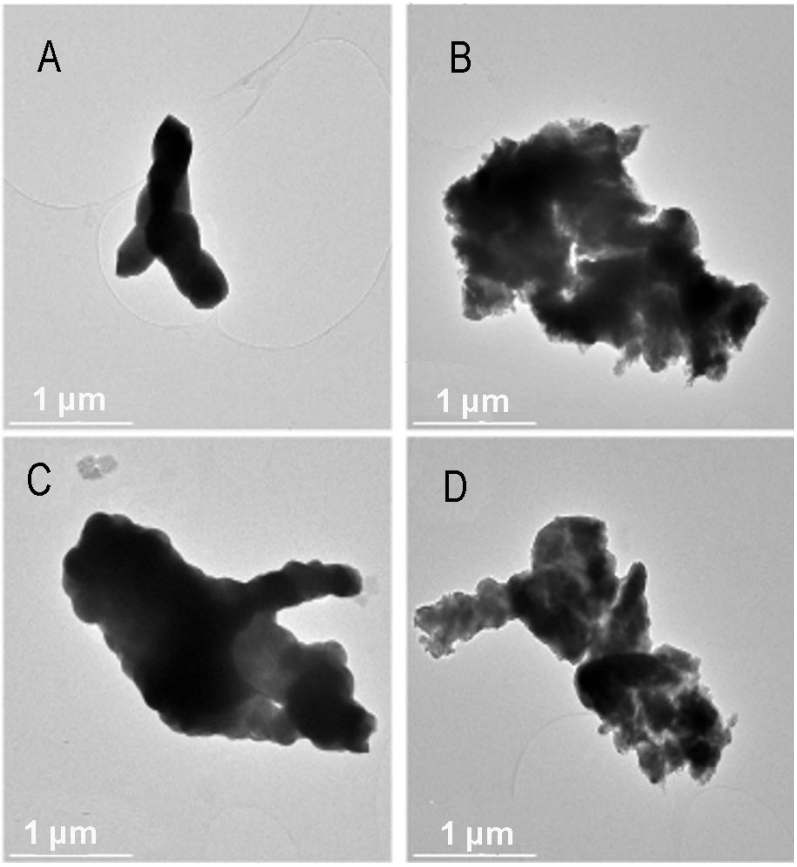

Figure S3: Transmission electron microscopy overview images of $La_{1.8}Ba_{0.2}NiO_4$ and $La_{1.8}Ba_{0.2}Ni_{0.9}Cu_{0.1}O_4$ in the initial (Panels A and C, respectively) and the DRM-spent state (Panels B and D, respectively).

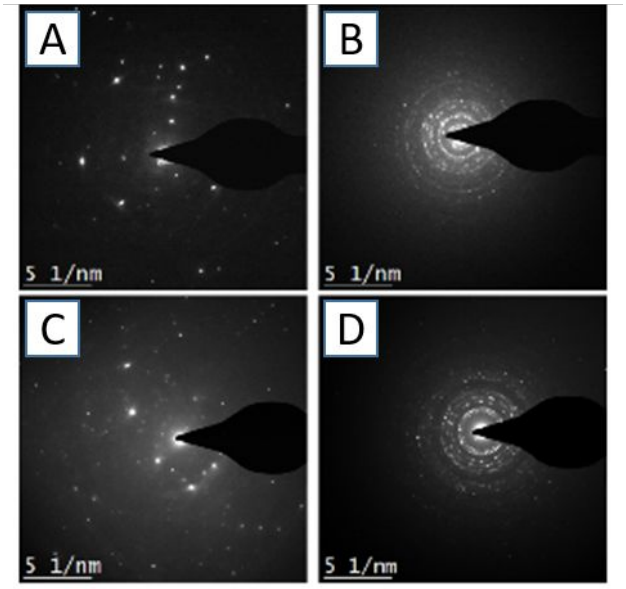

Figure S4: Selected area electron diffraction patterns of $La_{1.8}Ba_{0.2}NiO_4$ and $La_{1.8}Ba_{0.2}Ni_{0.9}Cu_{0.1}O_4$ in the initial (Panels A and C, respectively) and the DRM-spent state (Panels B and D, respectively).

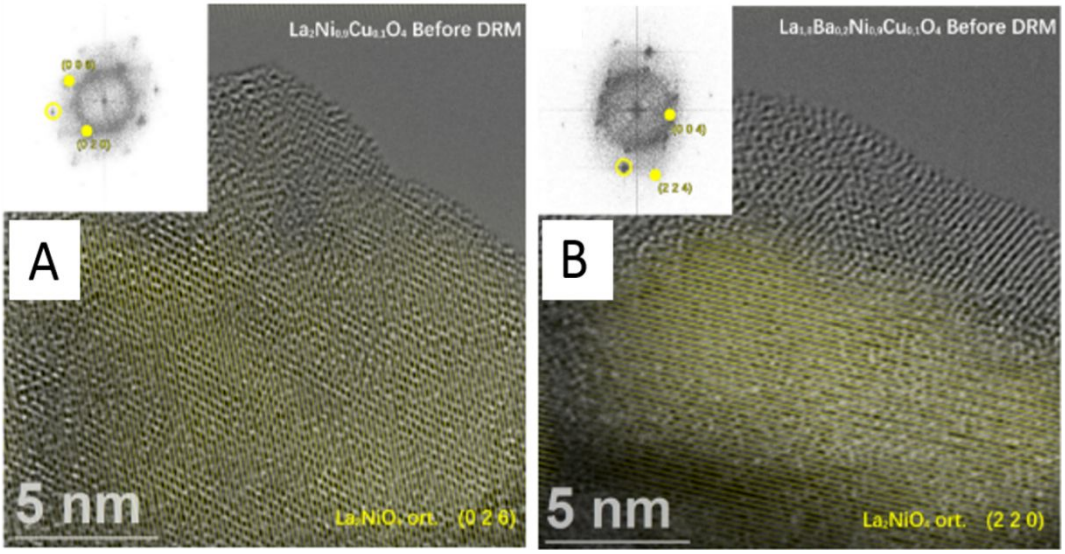

Figure S5: Aberration-corrected high-resolution electron microscopy images of $La_2Ni_{0.9}Cu_{0.1}O_4$ (Panel A) and $La_{1.8}Ba_{0.2}Ni_{0.9}Cu_{0.1}O_4$ (Panel B) in the initial state.

Representative lattice fringes of the orthorhombic La_2NiO_4 structure have been Fourier-filtered and accordingly color-coded to highlight the presence of individual grains.

Section C: Additional XRD analysis

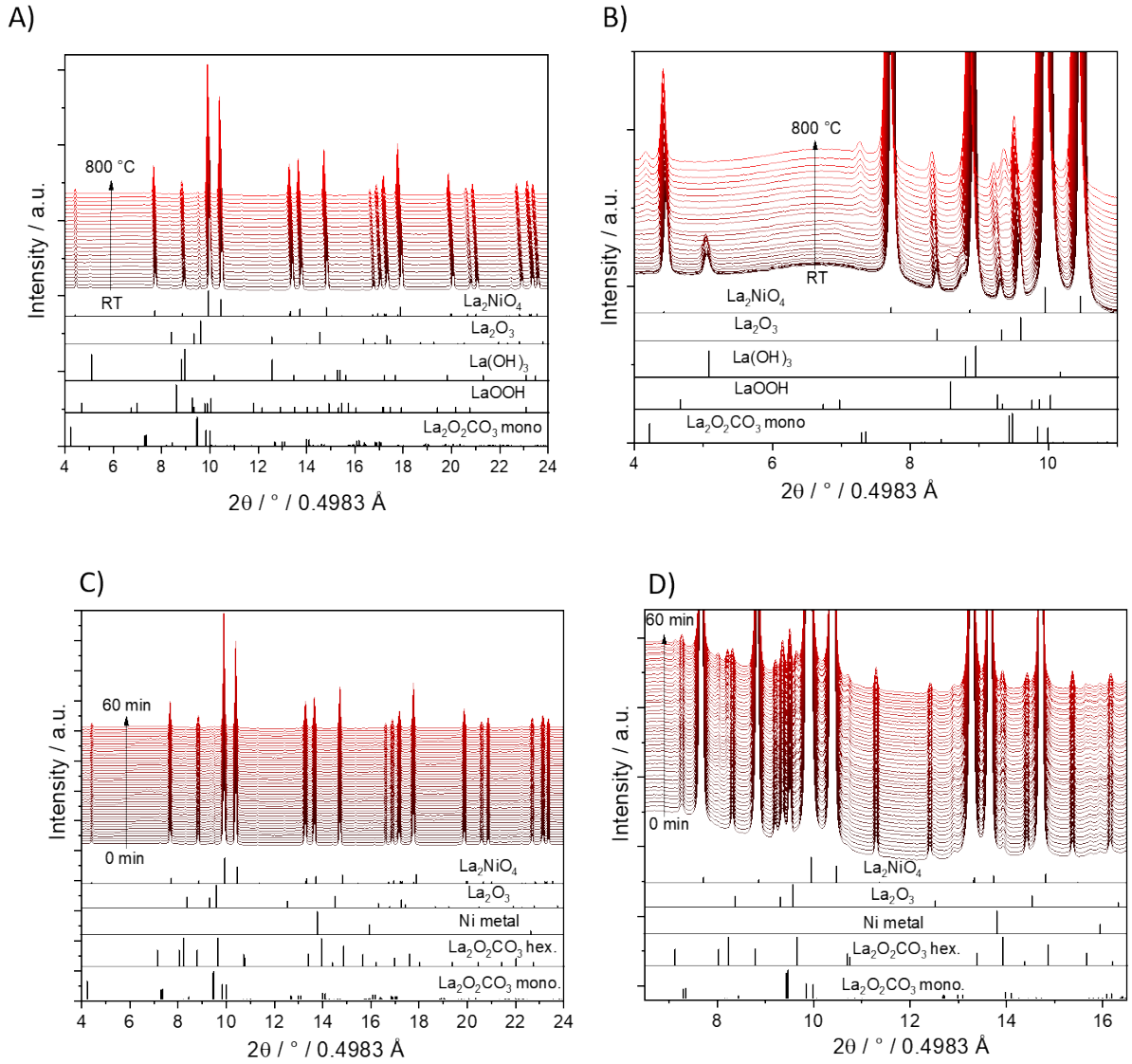

Figure S6: Panel A: *In situ* collected XRD patterns of $La_{1.8}Ba_{0.2}NiO_4$ during heating up to 800 °C under DRM conditions. Panels B focus on a narrower 2θ window for closer analysis. The lower panel indicates the phase assignment to the respective reference structures. Panel C: *In situ* collected XRD patterns of $La_{1.8}Ba_{0.2}NiO_4$ during holding at 800 °C for 60 min under DRM

conditions. Panels D focus on a narrower 2θ window for closer analysis. The lower panel indicates the phase assignment to the respective reference structures.

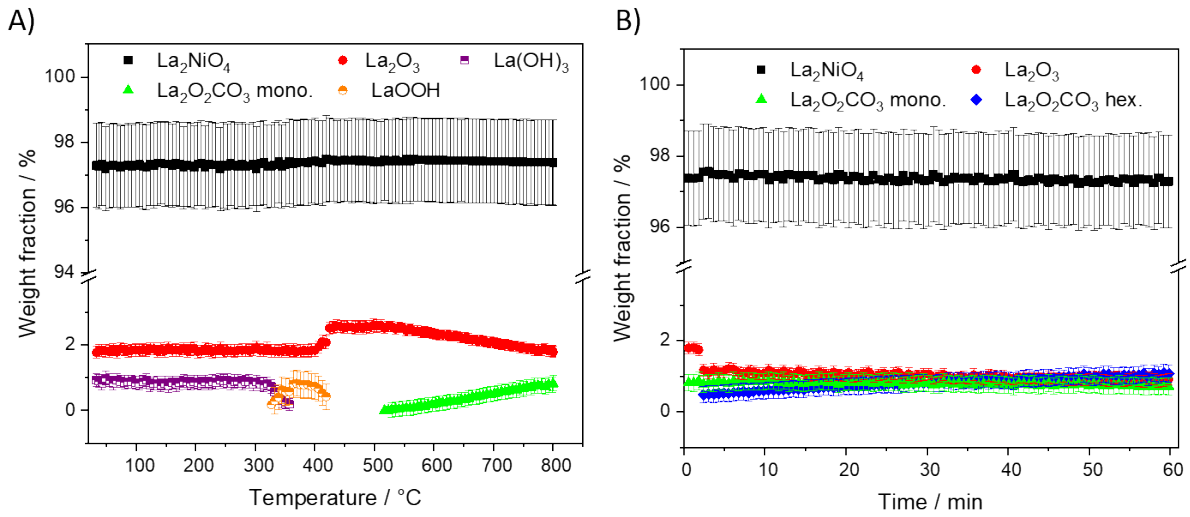

Figure S7: Weight fractions of different crystalline phases formed during DRM as a function of temperature (A) and time at 800 °C (B) obtained by Rietveld refinement of the *in situ* collected XRD patterns of $La_{1.8}Ba_{0.2}NiO_4$.

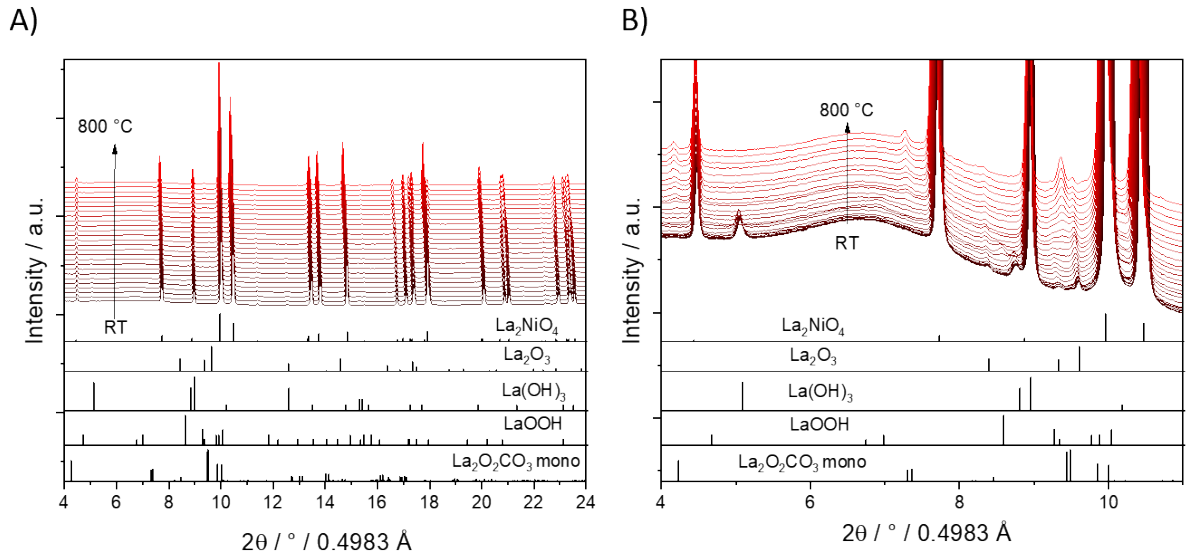

Figure S8: *In situ* collected XRD patterns of $La_2Ni_{0.9}Cu_{0.1}O_4$ during heating up to 800 °C under DRM conditions. Panels B focus on a narrower 2θ window for closer analysis. The lower panel indicates the phase assignment to the respective reference structures.

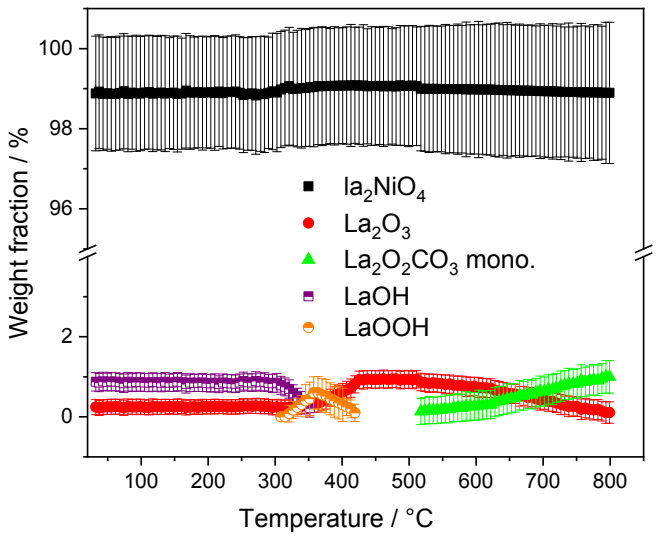

Figure S9: Weight fractions of different crystalline phases formed during DRM as a function of temperature obtained by Rietveld refinement of the in situ collected XRD patterns of $La_2Ni_{0.9}Cu_{0.1}O_4$.

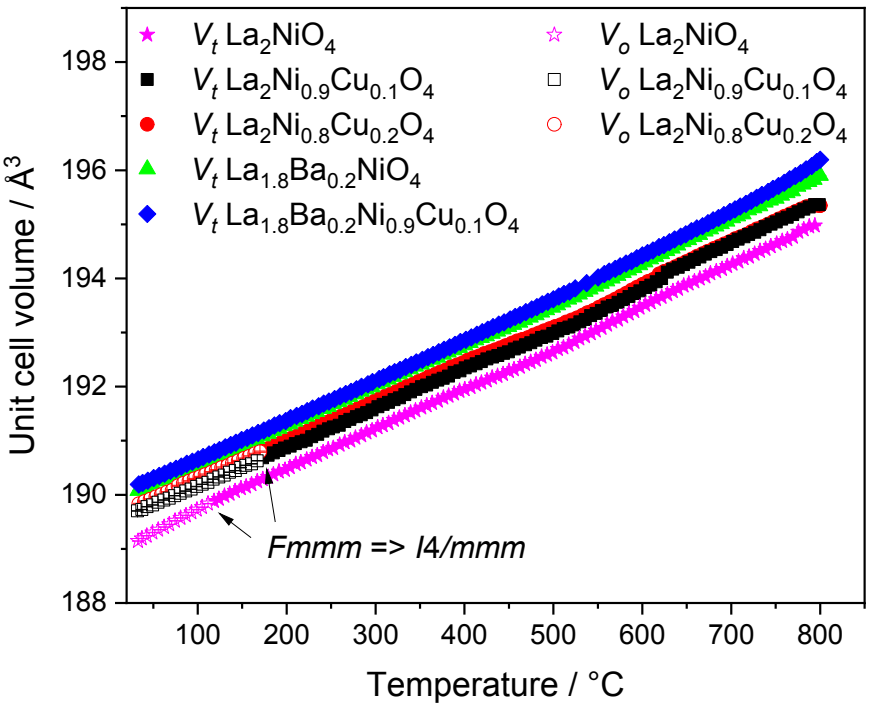

Figure S10: Evolution of the unit cell volume of pure and doped La_2NiO_4 samples as a function of temperature in the DRM mixture.

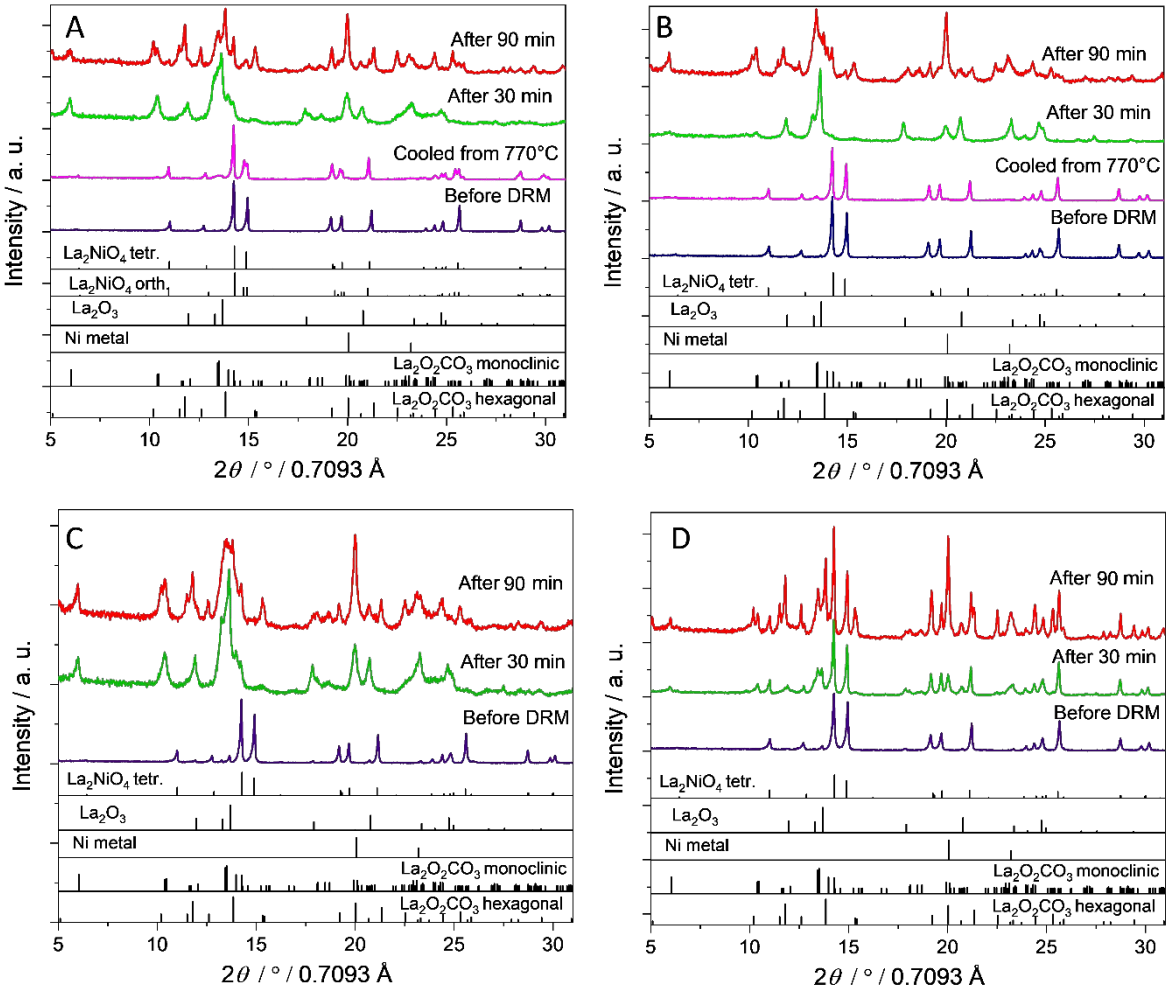

Figure S11: *Ex situ* collected PXRD patterns of $La_2Ni_{0.8}Cu_{0.2}O_4$ (A), $La_{1.8}Ba_{0.2}Ni_{0.9}Cu_{0.1}O_4$ (B), $La_2Ni_{0.9}Cu_{0.1}O_4$ (C), and $La_{1.8}Ba_{0.2}NiO_4$ (D) Ruddlesden-Popper materials before and after a catalytic DRM (CO_2:CH_4:He = 1:1:3) runs in a total gas flow of 100 mL min^{-1} at different conditions.

Section D: Additional XANES analysis

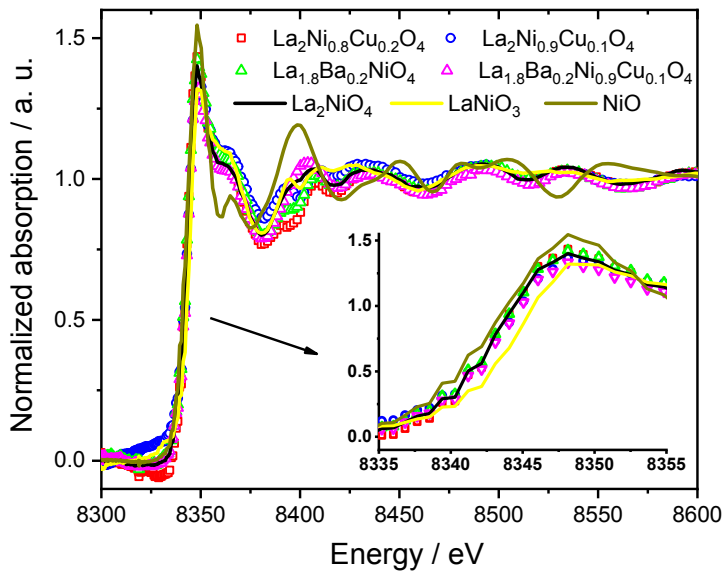

Figure S12: Normalized Ni *K*-edge X-ray absorption fine structure (XANES) of pure and doped La_2NiO_4 Ruddlesden-Popper materials as well of reference materials (NiO and $LaNiO_3$).

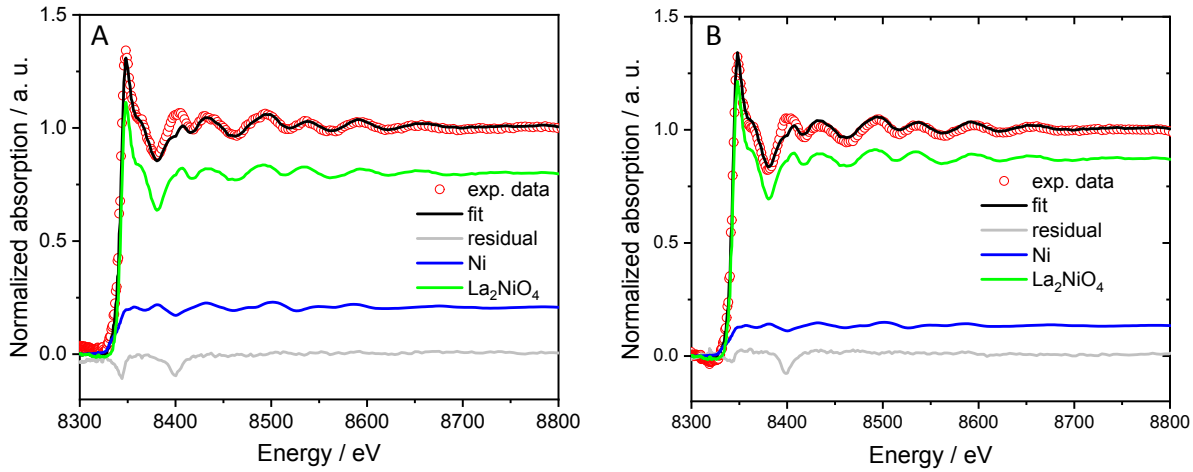

Figure S13: Linear combination fitting (LCF) of normalized Ni K-edge XANES spectra of $La_2Ni_{0.8}Cu_{0.2}O_4$ and $La_{1.8}Ba_{0.2}Ni_{0.9}Cu_{0.1}O_4$ with those of reference materials (NiO and La_2NiO_4).

Section E: XPS analysis

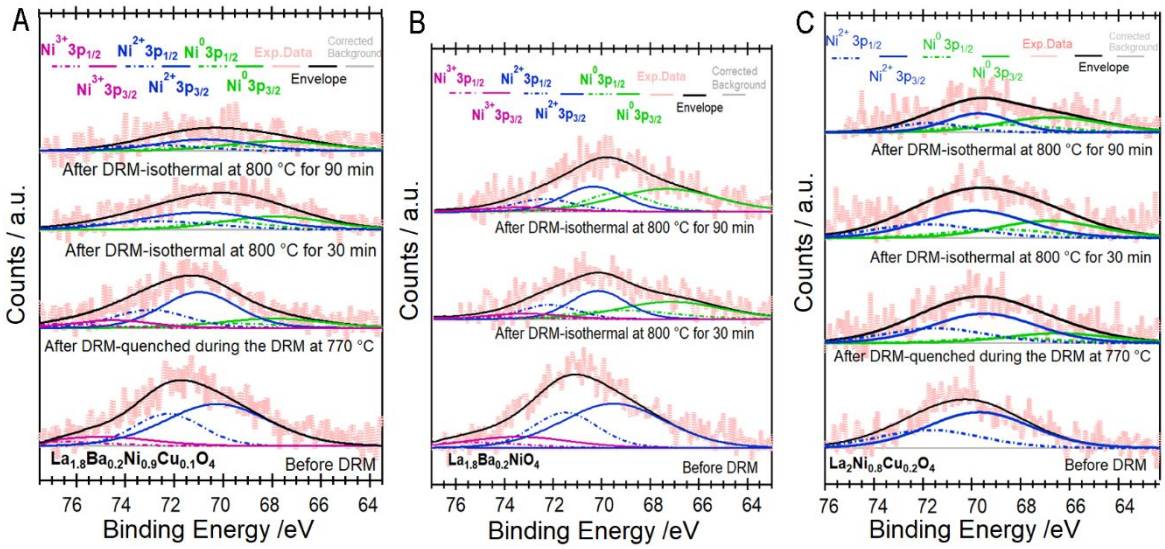

Figure S14: Full set of Ni 3p species of $La_{1.8}Ba_{0.2}Ni_{0.9}Cu_{0.1}O_4$ (Panel A), $La_{1.8}Ba_{0.2}NiO_4$ (Panel B) and $La_2Ni_{0.8}Cu_{0.2}O_4$ (Panel C) after selected DRM treatments.